MICROCOPY RESOLUTION TEST CHART

NATIONAL BUREAU OF STANDARDS-1963-A

AD A060100

ARACOR `ARO 14931. 3-MS`

LEVEL

SOLID-SOLID REACTIONS IN METAL FILMS ON SILICON

DDC FILE COPY

D D C
OCT 17 1978
RECEIVED
F

Prepared for:

U.S. ARMY RESEARCH OFFICE
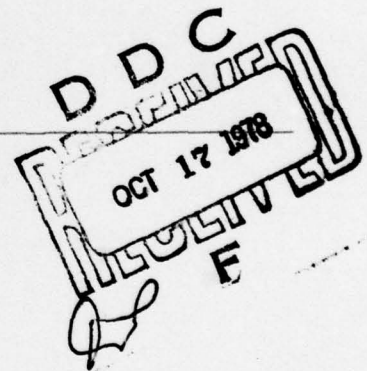
78 10 10 06

ADVANCED RESEARCH AND APPLICATIONS CORPORATION

C

6 SOLID-SOLID REACTIONS IN METAL FILMS ON SILICON

FINAL REPORT

ARACOR ~~REPORT NO.~~ FR-78-P6

10 T. J. Magee ~~and~~ J. Peng

14 ARACOR-FR-78-P6

12 50 p.

U.S. ARMY RESEARCH OFFICE

15 ARO-DAAG29-77-C-0024

9 Final rept. 1 May 77-30 Apr 78,

D D C
OCT 17 1978
F
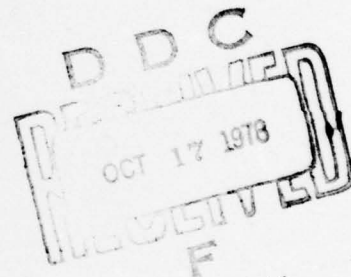
ADVANCED RESEARCH AND APPLICATIONS CORPORATION

11 14 Sep 78   18 ARO

19 14934.3-MS

APPROVED FOR PUBLIC RELEASE:
DISTRIBUTION UNLIMITED

78 10 10 063

393 004

CONTENTS

ACCESSION for

NTIS	White Section	☑
DDC	Buff Section	☐
UNANNOUNCED		☐
JUSTIFICATION		

BY
DISTRIBUTION/AVAILABILITY CODES

| Dist. | A.L. and/or SPECIAL | |
| A | | |

REPORT DOCUMENTATION PAGE		READ INSTRUCTIONS BEFORE COMPLETING FORM
1. REPORT NUMBER	2. GOVT ACCESSION NO.	3. RECIPIENT'S CATALOG NUMBER
4. TITLE (and Subtitle) SOLID-SOLID REACTIONS IN METAL FILMS ON SILICON		5. TYPE OF REPORT & PERIOD COVERED FINAL REPORT ~~26 APRIL 1976 TO 1 MAY 1978~~ *1 MAY 1977 - 30 APR 1978*
		6. PERFORMING ORG. REPORT NUMBER ARACOR PROJECT 6
7. AUTHOR(s) T. J. MAGEE AND J. PENG		8. CONTRACT OR GRANT NUMBER(s) ~~ARO~~ DAAG29-77-C-0024
9. PERFORMING ORGANIZATION NAME AND ADDRESS Advanced Research and Applications Corporation 1223 East Arques Avenue Sunnyvale, California 94086		10. PROGRAM ELEMENT, PROJECT, TASK AREA & WORK UNIT NUMBERS
11. CONTROLLING OFFICE NAME AND ADDRESS U.S. Army Research Office P. O. Box 12211 Research Triangle Park, NC 27709	12. REPORT DATE Sept. 14, 1978	13. NO. OF PAGES 42
	15. SECURITY CLASS. (of this report) Unclassified	
14. MONITORING AGENCY NAME & ADDRESS (if diff. from Controlling Office)	15a. DECLASSIFICATION/DOWNGRADING SCHEDULE	

16. DISTRIBUTION STATEMENT (of this report)

Approved for public release; distribution unlimited.

17. DISTRIBUTION STATEMENT (of the abstract entered in Block 20, if different from report)

18. SUPPLEMENTARY NOTES

The findings in this report are not to be construed as an official Department of the Army position, unless so designated by other authorized documents.

19. KEY WORDS (Continue on reverse side if necessary and identify by block number)

Silicon	Contacts
Thin films	Solid Phase Epitaxial Growth
Silicides	Electron microscopy
Metal-semiconductor reactions	Auger electron spectroscopy
Contacts	

20. ABSTRACT (Continue on reverse side if necessary and identify by block number)

Investigations were conducted on solid-solid reactions in gold and aluminum thin films formed on Si substrates at deposition temperatures below the eutectic points. Additional research was also performed on the reactions between Al thin films and polycrystalline (CVD) Si. As-deposited and annealed structures were studied using correlated data from transmission electron microscopy/diffraction (TEM/TED), Auger electron spectroscopy (AES) profiling, and forward current-voltage (I-V) measurements. Significant intermixing of Au/Si occurs within the Au film and diffusion of Au into the Si substrate occurs at temperatures >100°C.

DD FORM 1473
1 JAN 73

EDITION OF 1 NOV 65 IS OBSOLETE

19. KEY WORDS (Continued)

20 ABSTRACT (Continued)

Formation of silicides is initiated on the surface at grain boundary sites for temperatures $>100^{\circ}$C. From AES and TED data, the composition of the silicide has been identified as δ-Au_3Si. For extended anneals at temperatures $>330^{\circ}$C, additional silicides tentatively identified as the cubic alpha and gamma-phases have been detected. Correlated Schottky barrier-height measurements reflect the metallurgical changes occurring within mixing regions. Films deposited at temperatures $>100^{\circ}$C show a significant reduction in oxide coverage for air-annealed samples and samples aged at room temperature. Vacuum-annealed samples (deposited at temperatures $>100^{\circ}$C) show a reduction in subsequent intermixing, indicating the rate limiting effect of prior Au-Si mixing and silicide formation.

In a series of controlled experiments, it was found that Si within an Al film moves rapidly to grain boundaries of doped and undoped films on (100)Si substrates and forms epitaxial regrowth structures on these sites at the interface. The regrowth structures are highly defective, containing both stacking faults and dislocation lines. Dissolution zones on Si substrates with undoped films have been shown reproducibly to be nucleated at Al grains that contain excessively high microstructural defect densities, possibly introduced by stress accumulation in the Al film. The presence of interfacial impurities or thin discontinuous SiO_2 layers will also influence reactions at the Al/Si interface. However, under the present experimental conditions, the nucleation of dissolution zones and regrowth structures were shown to be related to Al film structure, thereby reducing the possibility of random nucleation associated with processing variations.

LIST OF FIGURES

LIST OF TABLES

1. INTRODUCTION

Reactions between deposited metal films and single or polycrystalline silicon substrates have received considerable attention in recent years because of immediate applications to integrated circuit fabrication. Numerous investigations have been conducted on the use of metal/semiconductor (M-S) systems in contact structures, diffusion sources, and silicon gate MOS technology. However, until recently, no detailed studies have been reported on M-S reactions regarding the influence of microstructure, grain boundaries, and interdiffusion initiation sites on the development of interfacial structures or on solid-phase regrowth mechanisms.

In this report, we present the results of studies[*] using correlated data obtained from transmission electron microscopy/diffraction (TEM/TED), scanning electron microscopy (SEM), Auger electron spectroscopy (AES) and current-voltage (I-V) measurements obtained on the Au-Si, Al-Si, and Al (polycrystalline)/Si (polycrystalline) systems. The results of these investigations have also led to the development of a tentative model that stresses the role of grain boundaries and microstructural defect nucleation sites in solid-phase regrowth of semiconductors from M-S structures.

---

[*]See list of publications.

1

2. SOLID-SOLID REACTIONS OF AU FILMS ON SILICON

The Au-Si system has been studied by a number of investigators.[1-5]
It has been established that at temperatures > 150°C (below the eutectic
temperature of 370°C), silicon migrates through Au thin-film layers and
accumulates on the surface in the form of silicon dioxide. The oxide
layer is nonuniform in thickness and its growth rate is influenced by both
the oxidizing ambient and the crystallographic orientation of the silicon
substrate. Recent results[5] obtained using Auger electron spectroscopy
profiling on the Au-Si structure subjected to extended vacuum anneals have
suggested that at temperatures > 200°C, Au reacts with Si to form thin-layer
(30Å) silicides at the surface. However, the composition of the silicides
was only inferred from Auger spectral line splitting and amplitude ratio
measurements. To date, no detailed studies have been undertaken of solid-
solid reactions within the Au film or substrate mixing zone at temperatures
significantly below the eutectic temperature. In this section, we present
the results of an investigation of Au-Si reactions using correlated data
obtained from transmission electron microscopy/diffraction (TEM/TED), Auger
electron spectroscopy (AES), and current-voltage (I-V) measurements.

2.1 Experimental Procedures

Polished, single-crystal Si wafers of (100) or (111) orientation obtained
from Semi Metals Corporation were used for this study. The samples were n-type
with resistivities ranging from 2.7 to 3.8 Ω-cm. The wafers were chemically
cleaned and immersed in a dilute hydrofluoric acid solution to remove surface
oxidation before depositing the Au thin films. Gold films ranging in thickness
from 100 to 1000-Å were deposited on the silicon surfaces at a vacuum level
of $\simeq 10^{-7}$ torr. Thickness of Au layers were measured by a quartz crystal
monitor during deposition and subsequently checked with a multiple-beam
interferometer after vacuum deposition.

Substrate temperatures were controlled by a sandwich-type heater and
temperature monitor. The substrate heater consisted of a Mo filament placed
between two quartz plates. During deposition, substrate temperatures were
maintained in the range of 25° to 200°C. Postdeposition thermal anneals were

done under vacuum or in air at temperatures up to 330°C for times varying from 5 min to 12 hr.

Annealed or "as-deposited" Au films were removed from the Si by dissolving the substrate in a solution of five parts HF and one part HNO_3. The film was removed from the solution with a 3-mm-diameter grid, and was subsequently rinsed and dried for TEM examination. In separate experiments, the Au film was stripped from the Si substrate using an aqua regia solution. The sample was then jet-thinned from the back surface for TEM/TED analysis of Si-Au interfacial and mixing regions of the substrate. Annealed samples were prepared for TEM by first immersing the speciment in a dilute HF solution and then exposing it to $(KI + I_2)$ and aqua regia solutions to remove SiO_2, Au + Si mixtures, and residual Au before jet thinning.

Since TED patterns from thin layers within interfacial or mixing zones are often obscure or ill-defined, it was necessary to develop a technique for clearly and reproducibly imaging diffraction data. Using a radiotoning procedure adapted from a technique described by Thackray et al,[6-8] we intensified electron diffraction patterns recorded on Ilford plates and obtained autoradiographs on secondary plates to reconstruct the intensified diffraction data. This procedure has proven effective in these experiments and other studies of interfacial transitional zones of heterojunctions and will be discussed in detail in a separate paper to be published.

Samples used for electrical measurements were coated on the back surface with a 1000-Å-thick Au-Sb film and alloyed at 450°C for 30 min prior to deposition of Au films. Gold dots, 1mm in diameter and 1000-Å thick, were vacuum-deposited on the front surface at substrate temperatures of 25°, 100°, and 160°C, respectively. After deposition, a number of samples were vacuum-annealed for 30 min at temperatures ranging from 150°C to 350°C. Air anneals were done in a tube furnace in the same temperature range.

Auger profiling of as-deposited and annealed structures was conducted in the vacuum chamber of an Auger spectroscopy unit obtained from Physical Electronics Inc. Single and dual Ar-ion sputtering guns were used to provide depth removal rates up to a maximum of 100 Å/min.

2.2 Results

2.2.1 Transmission Electron Microscopy/Diffraction

Transmission electron micrographs were obtained on Au thin films evaporated on Si wafers at substrate temperatures ranging from 25° to 190^oC. Representative bright-field electron micrographs are shown in Figures 1 and 2 for films evaporated at substrate temperatures of 100^oC and 150^oC, respectively. Average grain size measurements obtained from electron micrographs are summarized in Table 1.

Table 1

AVERAGE GRAIN SIZES IN Au FILMS EVAPORATED ON (100) Si WAFERS AS A FUNCTION OF Si SUBSTRATE DEPOSITION TEMPERATURE

Substrate Temperature (^oC)	Grain Size ($\overset{o}{A}$)
25	50 – 500
50	1000
100	2000 – 5000
150 – 160	<10,000
170 – 190	>10,000

The data in Table 1 indicate that Au grain size increases rapidly as a function of increasing substrate temperatures from 25° to 160^oC. At higher temperatures, the growth rate is substantially reduced, and apparent size saturation (≈1 μm) is obtained at temperatures below the Au-Si eutectic (370^oC).

In a number of films deposited at substrate temperatures > 100^oC, we observed thin discontinuous overlaying deposits nucleated selectively at grain boundaries. Since these deposits are relatively thin compared with the thickness of the Au film, it has been extremely difficult to identify the exact composition of the overlayer by TED. It is possible that gold silicides are formed preferentially at the grain boundary regions. AES profiling data tend to support the existence of thin silicide layers at the surface, as will be discussed in the next section.
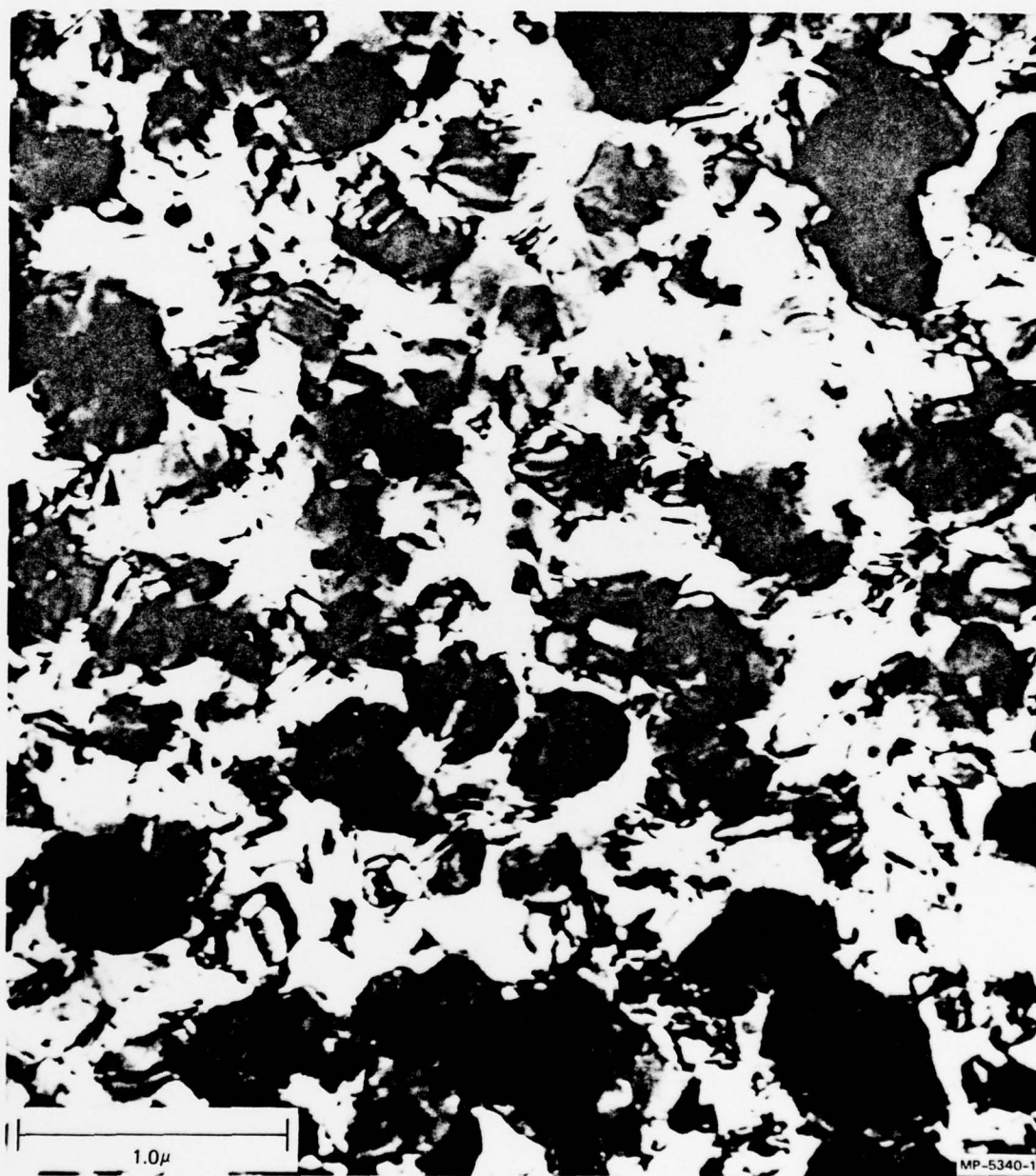
FIGURE 1. BRIGHT FIELD ELECTRON MICROGRAPH OF Au FILM EVAPORATED ON (100) SILICON AT SUBSTRATE DEPOSITION TEMPERATURE OF 100°C.

FIGURE 2. BRIGHT FIELD ELECTRON MICROGRAPH OF Au FILM EVAPORATED ON (100) SILICON AT SUBSTRATE DEPOSITION TEMPERATURE OF 150°C.

After the films were removed from the substrate with aqua regia, the as-prepared Si samples were thinned from the back surface for TEM analysis. Examination of interfacial and near-surface regions of the Si showed no detectable reactions or disordering of the lattice at substrate temperatures <100°C. At temperatures >100°C, diffraction patterns obtained from the mixing region exhibited a series of additional polycrystalline rings, as shown in Figure 3. Table 2 presents an analysis of data from this diffraction pattern and comparison with published data.[9] These data indicate that the second-phase crystallites are orthorhombic δ-gold silicide (Au_3Si) containing 17.9 atomic percent Si. Selected area electron diffraction patterns showed the presence of Au_3Si crystallites distributed throughout the Au-Si mixing region.

Au-Si structures prepared at variable substrate temperatures were annealed in a vacuum system at 10^{-7} torr to the eutectic point (≈370°C) of the Au-Si system. TEM examination of the Au films revealed that grain growth occurs rapidly on structures annealed at temperatures <200°C. Above anneal temperatures of 200°C, reordering is also observed at the top surface of the Au in the vicinity of grain boundaries. Mixing regions within the film and near-surface regions of the vacuum-annealed Au-Si structures were characterized by the presence of δ-phase gold silicide (Au_3Si) crystallites. The diffraction pattern and the analysis are shown in Figure 4 and Table 3, respectively. As the temperature and anneal time were increased, the number of crystallites and sharpness of diffraction rings also increased. In particular, the development of Au_3Si crystallites was readily detected in samples annealed for long intervals slightly below the eutectic temperature.

In contrast to the results obtained for vacuum-annealed structures, a thick SiO_2 layer develops on the surface of gold films of Au-Si structures annealed in air. The thickness of this layer is proportional to the initial thickness of the Au thin film and the annealing time, in agreement with previous results.[4]

Within the mixing region reactions are often complex resulting in the possible formation of more than one phase of gold silicide. The δ-phase was identified, although a number of weak diffraction rings were observed that could not be correlated with either the δ-phase, Si, or Au. In an earlier paper, Anantharaman et al,[10] identified two face-centered cubic intermetallic

7

FIGURE 3. TRANSMISSION ELECTRON DIFFRACTION PATTERN OBTAINED FROM MIXING ZONE OF Au/Si STRUCTURE. SUBSTRATE DEPOSITION TEMPERATURE = 150°C; NO POST DEPOSITION ANNEAL. DIFFRACTION PATTERN ENHANCED USING RADIOISOTOPIC TONING TECHNIQUES.
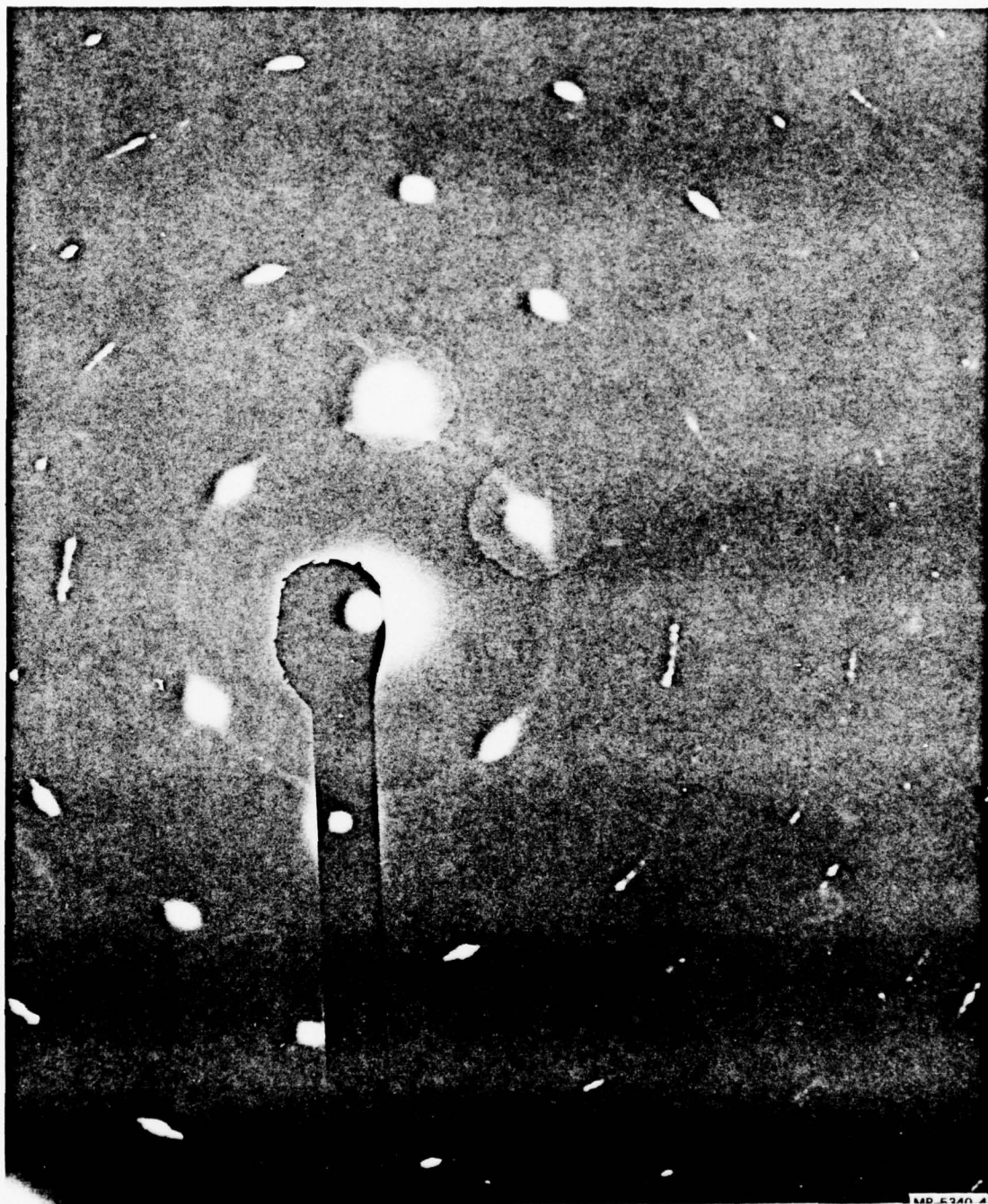
8

FIGURE 4. TRANSMISSION ELECTRON DIFFRACTION PATTERN OBTAINED FROM MIXING ZONE OF AN ANNEALED Au/Si STRUCTURE. SUBSTRATE DEPOSITION TEMPERATURE = 100°C; ANNEALED IN VACUUM FOR 30 MINUTES AT 330°C.

Table 2

ANALYSIS OF TRANSMISSION ELECTRON
DIFFRACTION PATTERN SHOWN IN FIGURE 3

Measured "d" Values	ASTM and Published "d" Values[*]	
	Si	δ Phase (Au$_3$Si)
3.195		3.195 (210)
3.116	3.116 (111)	
2.558		2.543 (301)
2.284		2.254 (220)
1.920	1.920 (220)	
1.637	1.638 (311)	
1.518		1.519 (126)
1.359	1.357 (400)	

_____

[*](hkl) values are given in parentheses.

Table 3

ANALYSIS OF TRANSMISSION ELECTRON
DIFFRACTION PATTERN SHOWN IN FIGURE 4

Measured "d" Values	ASTM and Published "d" Values[*]	
	Si	δ Phase (Au$_3$Si)
2.235		2.254 (220)
1.920	1.920 (220)	
1.368	1.359 (400)	
1.164		1.193 (228)
1.110		1.125 (440)
0.967	0.959 (440)	
0.888		0.874 (824)

_____

[*](hkl) values are given in parentheses.

phases of the Au-Si system, but unfortunately no detailed information was presented regarding indexing of the diffraction lines. We calculated "d" values of all possible reflections for the fcc lattice, using the published values for the lattice parameters of the α-phase (a = 7.84 Å) and the γ-phase (a = 19.50 Å). These data were then used to determine if measured "d" values obtained from diffraction patterns could be correlated with calculated values for the α-phases and γ-phases.

Figure 5 shows a representative diffraction pattern obtained within the mixing region of an Au-Si structure annealed in air at 400°C for 12 hr. Comparison of established and experimentally measured "d" values is shown in Table 4 and indicates good agreement for Si and δ-gold silicide lines. A number of additional lines can then be correlated with calculated d-values for the α- and γ-phases. However, the limited number of lines and the correlation with calculated rather than reported "d" values makes the identification of the α- and γ-phases very tentative. Since the appearance of more than one phase is noted within the mixing regions of all Au-Si structures annealed in air, we can assume formation of the orthorhombic δ-phase and at least one or more additional intermetallic silicides, possibly similar to the α- and γ-phases.

2.2.2 Auger Electron Spectroscopy

AES profiling analyses were obtained on "as-deposited" and vacuum- or air-annealed Au/Si samples as a function of temperature. Figures 6a to 6c show the results obtained on unannealed structures formed by vacuum deposition of Au at Si substrate temperatures of 25°C, 100°C, and 160°C, respectively. Figure 6a shows that room temperature deposition of the Au thin film produces no significant outdiffusion of Si into the Au layer. As the substrate temperature is increased (Figures 6b and 6c), Si diffuses rapidly into the Au film. At 100°C, Si has migrated to the surface of the Au and a mixed Au-Si film is formed. Similar experiments on structures annealed in vacuum at temperatures up to 330°C indicate that the amount of Si outdiffusion increases as the annealing temperature and annealing time increase. In all cases, there is a noticeable diffusion of Au into the Si substrate as a function of increasing substrate deposition and/or annealing temperature.

11

MP-5340-5

FIGURE 5.   TRANSMISSION ELECTRON DIFFRACTION PATTERN OBTAINED FROM
MIXING ZONE OF ANNEALED Au/Si STRUCTURE.   SUBSTRATE
DEPOSITION TEMPERATURE = 50°C; ANNEALED IN AIR FOR 12-HOURS
AT 400°C.

Table 4

ANALYSIS OF TRANSMISSION ELECTRON
DIFFRACTION PATTERN SHOWN IN FIGURE 5

Values (Å)	ASTM Published and Calculated "d" Values*			
	Si	α-Phase	γ-Phase	δ-Phase
5.540			5.629 (222)	
3.185	3.138 (111)			
3.049			3.083 (260)	
2.877		2.772 (021)		2.759 (020)
2.283		2.263 (222)		2.254 (220)
2.038			1.990 (844)	
1.915	1.920 (220)			
1.763		1.753 (420)		
1.636	1.638 (311)			
1.579				1.561 (107)
1.506				1.484 (430)
1.360	1.357 (400)			
1.289				1.272 (602)
1.234	1.246 (331)			
1.185				1.193 (228)

* (hkl) values are given in parentheses.

13
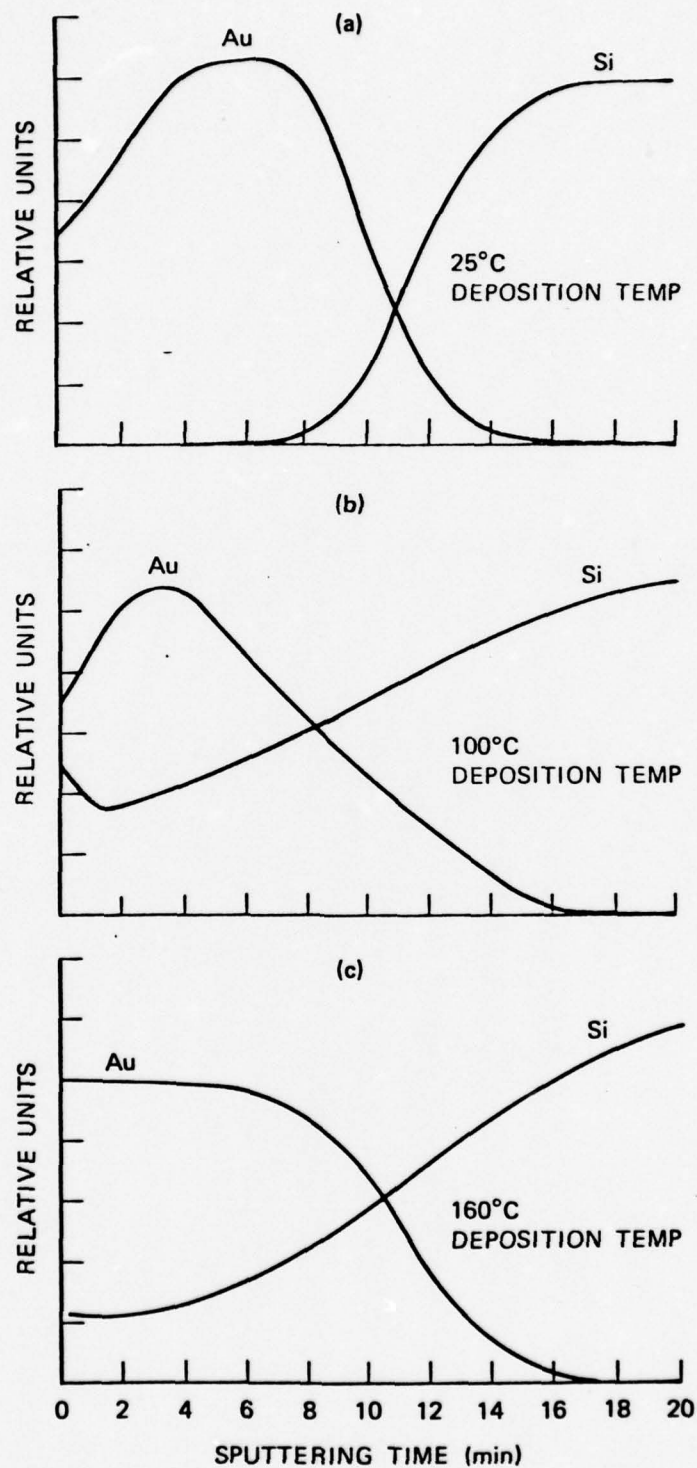
FIGURE 6   AES DEPTH PROFILES OF Au/Si STRUCTURES
PREPARED AT VARIOUS SUBSTRATE
DEPOSITION TEMPERATURES (NO ANNEAL)

14

Figures 7a to 7c show AES profiles for Au films that have been deposited on Si at Substrate temperatures of 25°C, 100°C, and 160°C, respectively, and annealed in air at 200°C. As the substrate deposition temperature is increased, significant intermixing of Si and Au occurs within the film and at the interface. The maximum near-surface concentration of oxygen is also present on films deposited at 20°C. At higher substrate deposition temperatures, the oxygen concentration is reduced, implying that the thickness of SiO_2 overlayers on Au/Si structures at moderate annealing temperatures is inversely proportional to the substrate temperature when the films were deposited.

We have also observed varying amounts of silicon and oxygen on the surfaces of films deposited at room temperature and allowed to age for several days in air. From AES profiles, the thicknesses of the oxide layers were determined to be $\simeq$ 200 Å for samples deposited at room temperature, $\simeq$ 50 Å for films deposited at 100°C, and $\leq$ 10 Å for layers deposited at 160°C.

For films deposited at room temperature, Si diffuses rapidly through the Au to accumulate at the surface. Annealing in air results in the formation of irregularly distributed oxides that reach a saturation thickness in proportion to the Au film thickness. Films deposited at substrate temperatures > 100°C exhibit a pronounced mixing phase and relatively inhibited growth of oxides at the surface. In addition, the mixed Au + Si phase within the film reduces room temperature thermal aging effects and the formation of oxides.

We observed two low-energy Auger peaks that can be associated with the formation of silicides in as-deposited and vacuum-annealed (200°C, 30 min) films deposited at 25°C. These were positioned at 85 eV and 88.5 eV and are attributed to the splitting of the Si-LVV peak at 92 eV. In agreement with Green and Bauer,[5] we observed an apparent silicide thickness of $\simeq$ 35 Å at the surface of the film. However, our data indicate that the probable composition of the silicide in Au_3Si, as confirmed in direct identification from electron diffraction plates using radioisotopic image enhancement techniques.

2.2.3 Electrical Measurements

The forward current-voltage characteristics will be particularly sensitive to the development of interfacial reactants or transitional layers at the metal-semiconductor interface. For comparison and correlation with
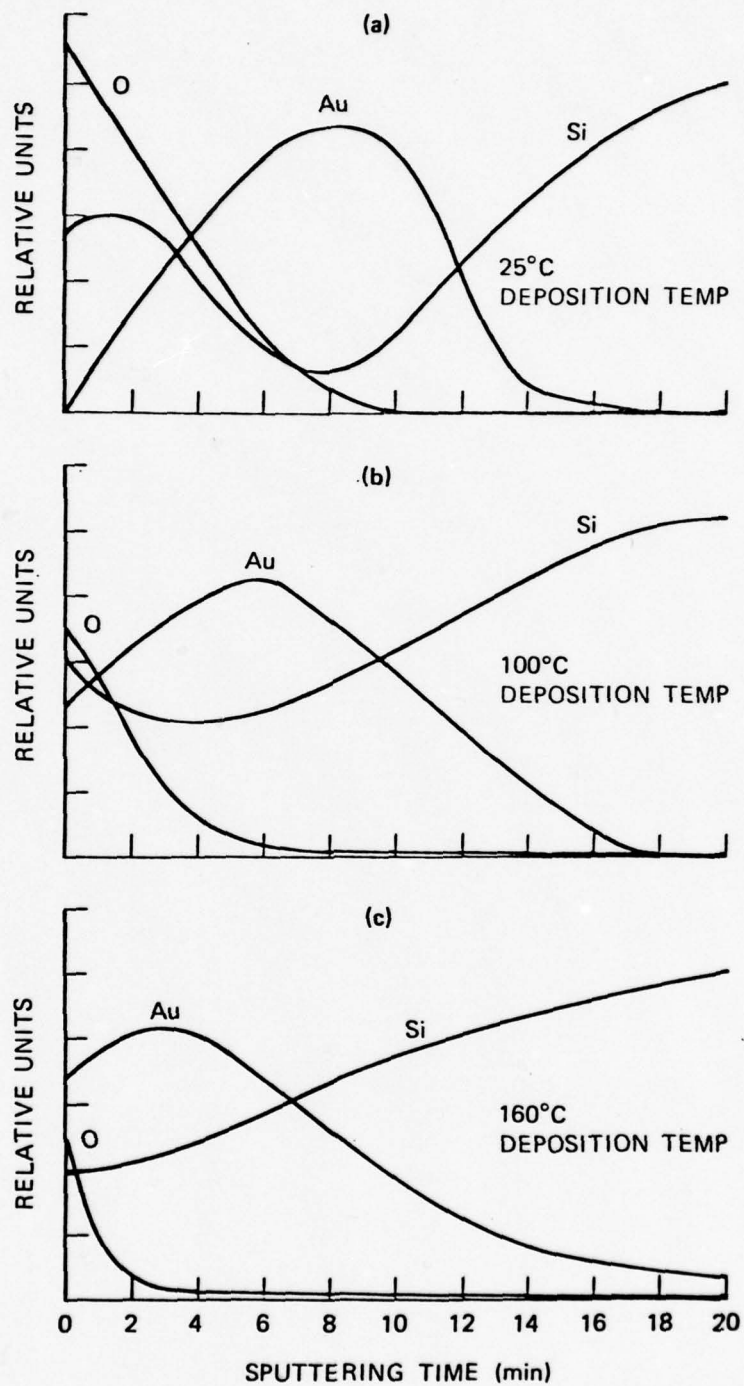
FIGURE 7   AES DEPTH PROFILES OF 200°C AIR ANNEALED
(30 MINUTES) Au/Si STRUCTURES PREPARED AT
VARIOUS SUBSTRATE DEPOSITION TEMPERATURES

the results discussed in the previous section, we show in Figures 8 to 10 the I-V characteristics for samples prepared under various substrate deposition and annealing conditions.

The thermionic emission theory for charge transport in Schottky barrier structures describes the barrier height, Φ_B, in the following equation:[11]

$$\Phi_B \simeq \frac{kT}{q} \ln \frac{A^{**} T^2}{J_s} \tag{1},$$

where k is Boltzmann's constant; A^{**} is the effective Richardson constant; and J_s is the saturation current density. If the forward current is extrapolated to the current axis on an $\ln I_f$ vs. V_f plot, the intersection on the axis defines the saturation current in the relation, $I_s = J_s A$, where A is the metallurgical area of the contact. Using (1), the value of Φ_B can then be determined. However, this approach must be used cautiously since (1) is valid only in the pure thermionic emission region for moderately doped substrates when the ideality factor $\simeq 1$ and where the empirical approach yields the smallest percentage error in the value of Φ_B.[12]

Under these restrictions, we determined approximate barrier heights from Figure 8 for films deposited at $25^{\rm o}$C and $100^{\rm o}$C to compare with results reported earlier in similar experiments. The barrier height for the Au film deposited at $25^{\rm o}$C is $\simeq 0.81$ eV, in reasonable agreement with previously published results. At a deposition temperature of $100^{\rm o}$C, $\Phi_B \simeq 0.77$ eV, reflecting the initial development of the interdiffusion regions and thin interfacial layers on the substrate. For films deposited at $160^{\rm o}$C, the I-V characteristics show that the ideality factor departs significantly from 1.00 and the possible error in determining Φ_B using the extrapolated slope method can be large.[12] In all cases, we observe a significant displacement in the forward I-V characteristics at lower voltages as the deposition temperature is increased from $25^{\rm o}$C to $160^{\rm o}$C, reflecting the development of prominent Au-Si mixing phases and the transition from thermionic emission toward field-emission-dominated conduction.

The effect of $200^{\rm o}$C vacuum annealing on the charge transport properties of films deposited at variable substrate deposition temperatures is shown in Figure 9. As the substrate temperature is increased from $25^{\rm o}$C to $160^{\rm o}$C, the
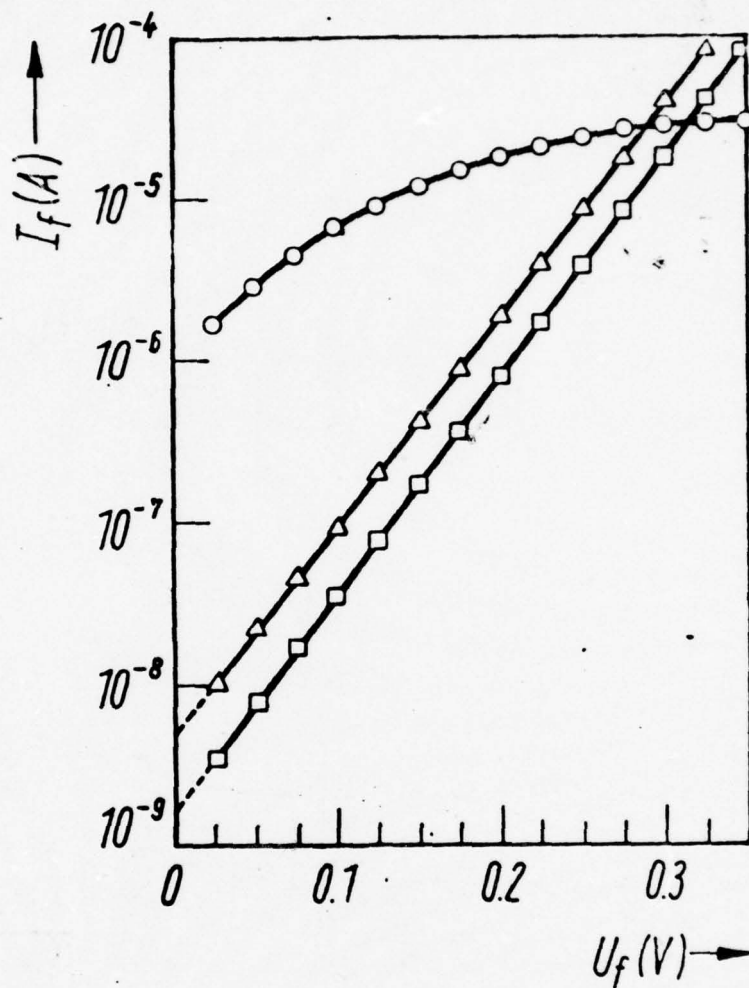
17

FIGURE 8. FORWARD CURRENT-VOLTAGE CHARACTERISTICS OF Au
FILMS DEPOSITED ON (100) Si AT VARIABLE SUBSTRATE
TEMPERATURES (NO POST ANNEAL). □ sample 1AD, T_{dep} =
25°C; △ sample ZAD, T_{dep} = 100°C; O sample 3AD,
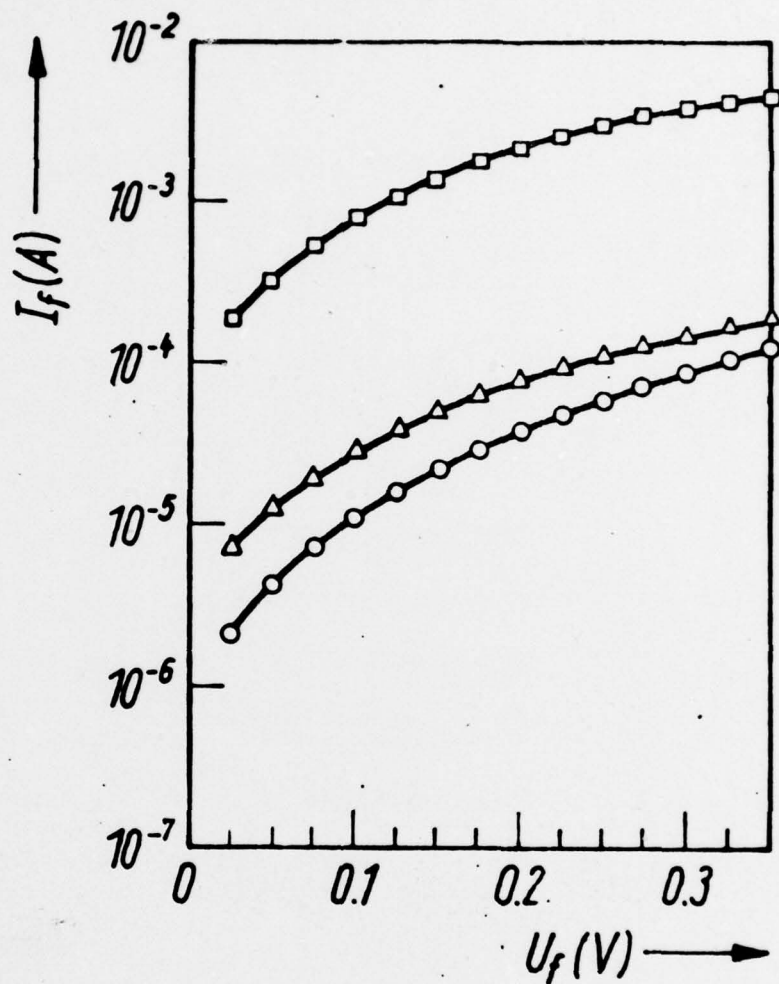T_{dep} = 160°C.

18

FIGURE 9. FORWARD CURRENT–VOLTAGE CHARACTERISTICS of 200°C
VACUUM ANNEALED (30 MINUTES) Au FILMS DEPOSITED
ON (100) Si AT VARIABLE SUBSTRATE TEMPERATURES.
$\square$ sample 1V, T_{dep} = 25°C; $\triangle$ sample 2V, T_{dep} = 100°C
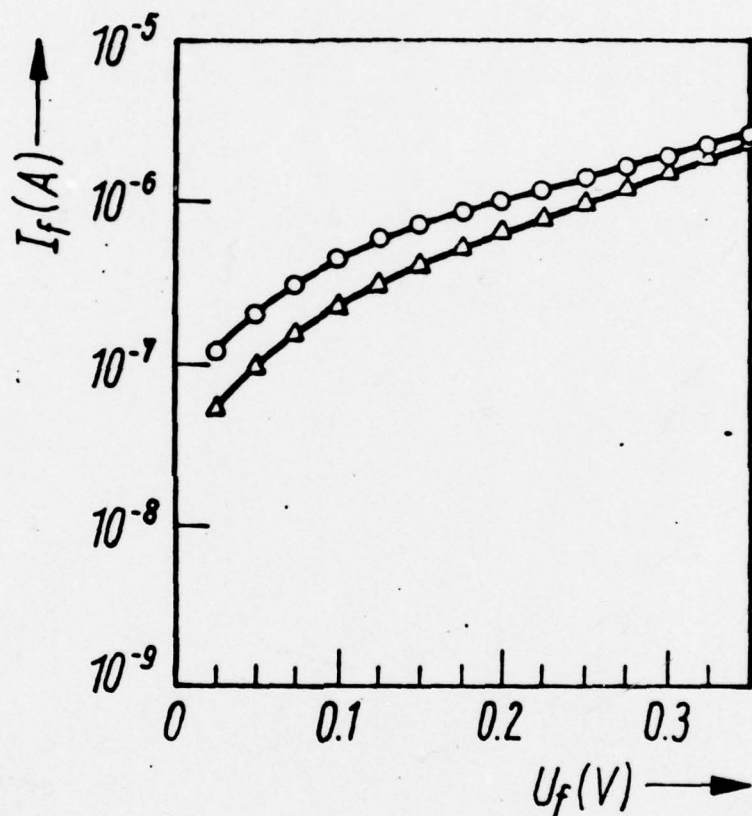O sample 3V, T_{dep} = 160°C.

FIGURE 10. FORWARD CURRENT-VOLTAGE CHARACTERISTICS OF 200°C
AIR ANNEALED (30 MINUTES) Au FILMS ON (100) Si AT
VARIABLE SUBSTRATE TEMPERATURES. Δ sample 1A, T_{dep} =
100°C; O sample 2A, T_{dep} = 160°C.

20

forward current also exhibits a pronounced increase relative to unannealed samples deposited at temperatures <160°C. The most pronounced variation, however, occurs for annealed samples deposited at 25°C. On these samples, the forward current increases several orders of magnitude after annealing, corresponding to the development of a highly mixed region within the film and an apparent deep indiffusion of Au into the substrate. Correlated AES and TED data indicate that prominant mixing and silicide formation occur during deposition at substrate temperatures >100°C. The I-V characteristics then suggest that the prior formation of Au-Si mixing regions and the subsequent motion of Au into the Si substrate during deposition will inhibit the outdiffusion of Si and subsequent motion of Au into the Si substrate during annealing. This conclusion is further supported by the similarity of I-V characteristics for as-deposited and annealed samples deposited at 160°C.

In contrast to the results obtained for vacuum-annealed samples, structures annealed in air at 200°C develop varying thicknesses of SiO_2 films at the surface. Samples deposited at 25°C and annealed at 200°C exhibit relatively thick discontinuous SiO_2 films on the surface, and the I-V measurements show a large amount of variability, depending upon the uniformity and lateral coverage of the oxide. At deposition temperatures $\geq$100°C, oxide layers on the annealed samples are relatively thin, as indicated in AES and TED experiments. The I-V plots are shown in Figure 10 for air-annealed samples deposited at 100°C and 160°C. In comparison to the results shown in Figure 9, the forward currents are somewhat lower for air-annealed samples, implying that the thin oxide layers at the surface are dominating injection at the contact probe.

2.3 Conclusions

In this study, we have shown that the grain size of Au films formed at variable substrate deposition temperatures on Si substrates increases from 50 Å to 500 Å at room temperature to an apparent size saturation of $\simeq$ 1 μm at temperatures >170°C. At substrate deposition and/or anneal temperatures $\geq$100°C, the orthorhombic δ-gold silicide (Au_3Si) is detected within the mixing region. The initial phases of growth is observed at the AuSi interface and

21

within thin ($\approx$35 Å thick) zones at the surface of the Au film. Correlated TEM and AES results suggest that the growth of the silicide is initiated preferentially at grain boundary sites. At higher anneal temperatures ($\geq$330^{o}C), the appearance of the δ(Au$_3$Si) phase and at least one or more additional intermetallic silicides, possibly similar to the x- and γ-phases, is noted throughout the film.

At substrate deposition or vacuum anneal temperatures >100°C, Si out-diffuses readily into the Au film, producing a heavily-mixed Au-Si region and Au indiffusion. Annealing in air produces similar Au-Si mixing zones and a discontinuous SiO$_2$ surface layer that increases in thickness as the Au film thickness increases. Growth of the oxide layer in annealed films deposited at substrate temperatures $\geq$100°C, however, is inhibited by the formation of mixing regions and silicides. In like manner, the development of oxide films during room temperature aging is more pronounced for films deposited at 25°C and is negligible for films deposited at temperatures >100°C.

Correlated I-V measurements on samples deposited at variable substrate temperatures and annealed in vacuum or air below the eutectic temperature, also reflect the metallurgical changes occuring within the Au film and at the Au-Si interface. At deposition (or vacuum anneal) temperatures $\geq$100^{o}C, the development of prominent Au-Si mixing zones yields a reduction in Schottky barrier height and a marked increase in forward current. Samples deposited at 25^{o}C and subsequently annealed in vacuum at 200^{o}C exhibit a larger increase in forward current than those deposited at higher temperatures. The results indicate that the formation of silicides and intermixing regions during deposition will be rate-limiting for additional metallurgical changes during post-deposition annealing. In contrast, samples annealed in air will exhibit variable I-V characteristics relative to the vacuum annealed samples, reflecting the varying thickness and discontinuity of SiO$_2$ layers at the surface of air annealed Au-films.

22

3. SI EPITAXIAL REGROWTH AND GRAIN STRUCTURE OF ALUMINUM METALLIZATION ON SINGLE CRYSTAL $\langle 100 \rangle$ SI

The interaction between Al films and single crystal or polycrystalline Si substrates has received considerable attention[13-17] in recent years because of numerous applications to integrated circuit technology. Silicon is known to dissolve in Al thin films at temperatures below 577°C, producing pitted surfaces and diffusion into shallow junctions. Additions of Si to the Al film will suppress dissolution of the substrate,[18] however, excess Si in the film will form precipitates at the Al/Si interface.[13,19] Generally, the solid-phase regrowth regions observed within the Al/Si system are in the form of large "mesa" structures of p-type silicon on a thin, relatively uniform p-type Si layer. Interfacial growth structures resulting from heat treatment of thick Al films on Si substrates of $\langle 111 \rangle$ orientation often show no correlation with Al grain structure[14] and dissolution pits are reported to occur randomly at a Si surface. However, it has recently been suggested that Si growths occurring out of an Al metallization may relate both to orientations of the Al grains and to orientation of the Si substrate.[15]

During the past year, a series of experiments were conducted to provide a more detailed investigation of Si regrowth on Si (single crystal wafers) and to investigate the formation of dissolution pits and regrowth structures in relation to Al grain structure.

In this study, polished Si wafers (n type, 2 Ω-cm) of $\langle 100 \rangle$ orientation ($\pm 1°$) were used. Surfaces were cleaned with organic solvents, rinsed in deionized (DI) water, followed by immersion in a dilute hydrofluoric acid solution and a final DI rinse. After drying, samples were immediately placed in an oil-free vacuum system and 1-μm-thick Al depositons done at vacuum levels less than 10^{-7} Torr. Al films were formed by e-beam evaporation and doped Al films deposited by sputtering from Al targets containing 2% Si. Subsequently, the Al/Si samples were annealed in a flowing N_2 atmosphere in the temperature range, 450° to 550°C, for periods between 10 min and 1 hr. The samples were cooled at $\simeq$ 3°C/min to $\simeq$ 100°C and then rapidly quenched to room temperature.

After heat treatment, a number of samples were prepared for TEM analysis

of film microstructure by conventional jet thinning at the back side of the Al/Si structure. The thinning was carefully controlled by observing the thinned region under a microscope. The thinning was terminated just before the Al film was reached, leaving the Al film intact over the etched Si substrate. In separate experiments, the Al films were removed by immersing the samples in a dilute hydrochloric acid (HCl) solution. The samples were first examined by SEM and the same specimens subsequently prepared for TEM by jet thinning. AES analyses were performed at an initial vacuum of less than 10^{-10} Torr using dual Ar-ion sputtering guns to provide a maximum layer removal rate of $\simeq 100$ Å/min.

In Figure 11, we show representative SEM data obtained at the interface of Al (undoped)/Si samples hearted to 550°C for 45 minutes and cooled at $\simeq 3^{\circ}$C/minute. After brief immersion in a dilute HCl solution, remnants of the Al film were retained at particular locations on the Si wafer. Energy dispersive x-ray analyses within the microscope showed that these selected regions were rich in Si and that substantial penetration of Al into the substrate had occured at these zones. In Figure 11a, undercutting at the edges of the particles reveals nucleation sites for dissolution pitting or faceting of the [100] Si surface. Additional exposure in the HCl solution removed the Si/Al interdiffusion zones (Figure 11b), leaving the pitted areas exposed on the substrate for observation. Dissolution pit depths were measured in the range 0.1 μm to 0.5 μm, in agreement with AES profiling experiments that indicated penetration of Al to comparable depths in the Si substrate.

Of particular interest in Figure 11 is the correlation between pitted areas and regrowth structures. The regrowth structures are observed in the form of lineated or tetrahedral "hillocks" (average height $\simeq$ 0.1 μm) that provide an outline of the Al grain structure on the Si substrate. Interestingly, the dissolution pits were not randomly oriented on the Si surface, but occurred repeatedly beneath the sites of individual Al grains. This conclusion is further substantiated by TEM analysis of the Si substrates.

In Figure 12, the bright-field transmission electron micrograph obtained on the Si substrate again shows the presence of regrowth structures at the interface and dissolution pits within the area defined by the outline of the grain structure. Selected area diffraction patterns obtained at hillock sites
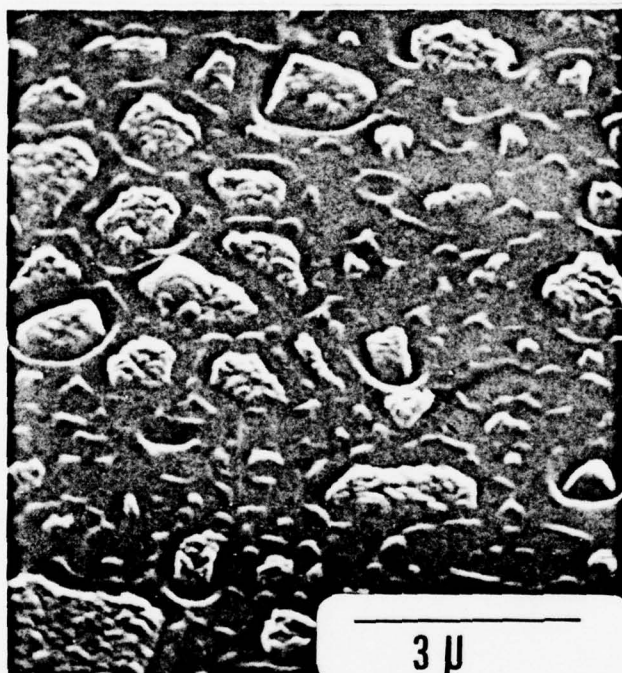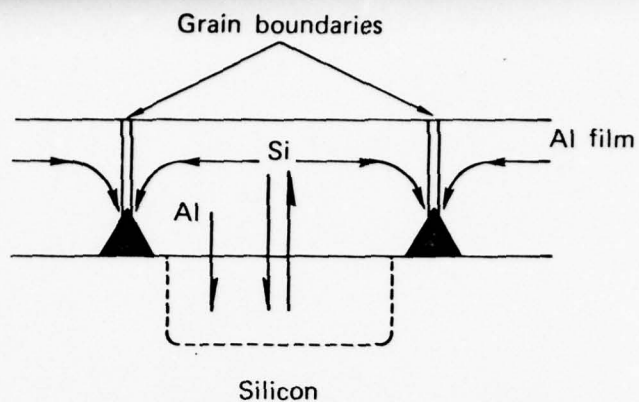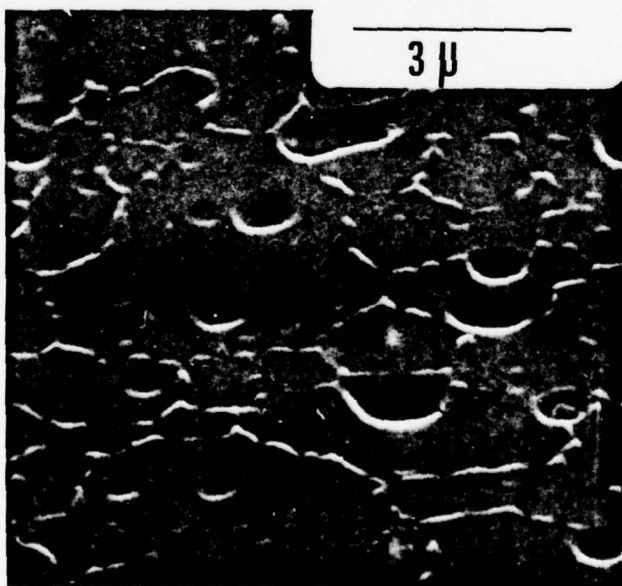
24

FIGURE 11. SCANNING ELECTRON MICROGRAPHS OF Si SUBSTRATE AFTER REMOVAL OF EVAPORATED (UNDOPED) Al FILM. a) SHORT HCl IMMERSION, b) EXTENDED HCl IMMERSION.

25

FIGURE 12.   BRIGHT-FIELD TRANSMISSION ELECTRON MICROGRAPH OF Si
SUBSTRATE AFTER REMOVAL OF (UNDOPED) Al FILM.

also confirmed that the regrowth structures were single crystal Si. However, careful TEM examinations of the microstructure of individual sites indicated that the regrowth sites were highly defective, containing both dislocation lines and stacking faults.

To provide further information on the correlation between grain structure and dissolution pitting, we used TEM to examine Al film structure in the regions immediately over dissolution pits. Al grains (1 to 3 μm average size) overlying dissolution zones were shown to contain Si precipitates ($\simeq$ 200 Å diameter) and large dislocation line densities. In all cases, dissolution zones are not observed beneath grains containing substantially lower defect densities. In agreement with SEM data shown in Figure 11, dissolution zones were observed within (defective) grain sites with no significant development at grain boundaries.

It is possible that the excess defect density observed within grains can be related to stresses generated in the Al film as a result of varying thermal expansion between Si and Al, in general agreement with the stress hypothesis proposed by Sankur et al.[14] In this case, the presence of large concentrations of dislocation lines would contribute both to the enhanced indiffusion of Si into the Al grain and lateral transport of Si to grain boundaries during cooling. Since grain growth (size) was shown to saturate at heating times < 30 minutes, the presence of a larger number of smaller grains and boundaries during the early stages of annealing will also contribute to the enhancement of Si motion into the Al film due to the high diffusivity of Si along the grain boundary channels.

For comparison, we performed an identifcal set of experiments on sputter-deposited Al films containing 2% Si. SEM examination (Figure 13) shows a similar epitaxial regrowth (average height $\simeq$ 1500 Å) at grain boundaries. Average grain size (after heating/cooling) determined from correlated TEM and SEM data was $\simeq$ 0.4 μm. The smaller initial grain size resulted in a relatively larger number of boundaries and regrowth structures for the sputtered films when compared to results obtained for evaporated films. Neither SEM examinations nor AES profiling experiments showed evidence of Al indiffusion or dissolution within the Si substrates, as anticipated. TEM analysis of interfacial structures additionally indicated that the regrowth regions were highly faulted, in agreement with results presented in the previous paragraphs.
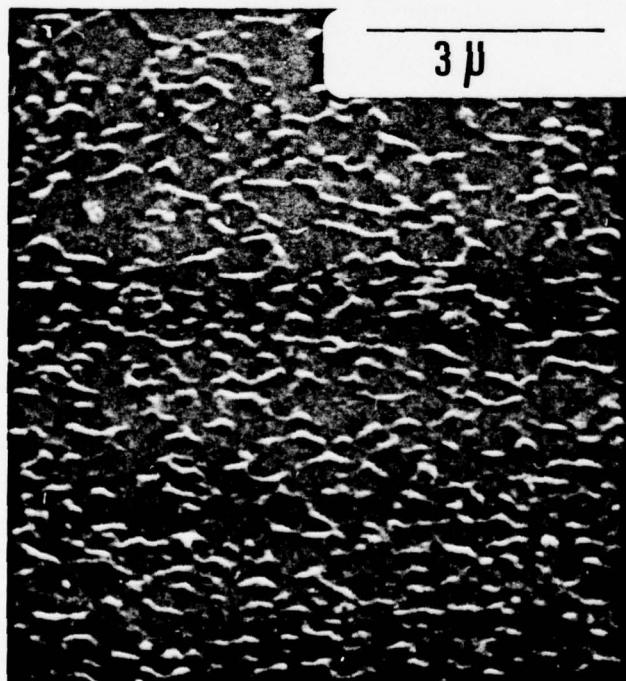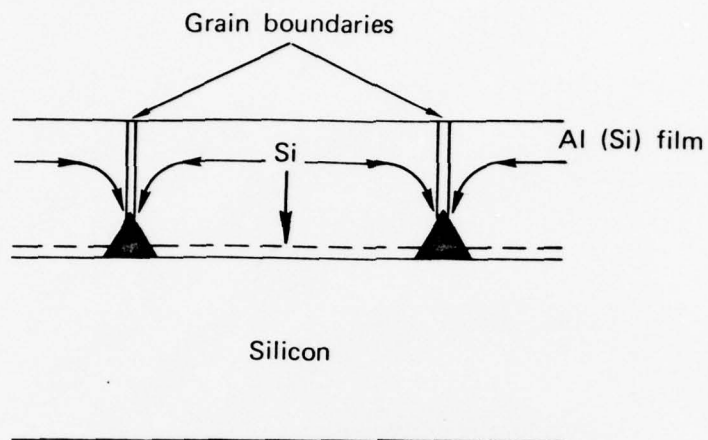
27

Grain boundaries

Al (Si) film

Si

Silicon

FIGURE 13.   SCANNING ELECTRON MICROGRAPH OF Si SUBSTRATE AFTER
REMOVAL OF SPUTTERED Al (2% Si) FILM.

28

At longer annealing times (greater than 1 hr), regrowth structures at the interface are often more complex. In contrast, films heated at 550°C for times of 10-45 min. show well-defined regrowth structures at grain boundaries. It is conceiveable that at longer heating times, a larger concentration of defects will be produced in the film, providing an increase in the number of trasnport paths for Si motion. During cooling, regrowth will proceed rapidly at grain boundaries producing slightly larger, irregular structures and increased lateral coverage at the interface.

In conclusion, we have shown in a series of controlled experiments that Si within an Al film moves rapidly to grain boundaries of doped and undoped films on [100] Si substrates and forms epitaxial regrowth structures on these sites at the interface. The regrowth structures are highly defective, containing both stacking faults and dislocation lines. Dissolution zones on Si substrates with undoped films have been shown reproducibly to be nucleated at Al grains that contain excessively high microstructural defect densities, possibly introduced by stress accumulation in the Al film. The presence of interfacial impurities or thin, discontinuous SiO_2 layers will also influence reactions at the Al/Si interface.[15] A recent paper[20] has also suggested that the nucleation of regrowth structures may proceed from local defect sites with the native SiO_2 layer ($\simeq$ 30 Å thick). However, under such conditions, dissolution zones and regrowth structures would be randomly distributed on the Si substrate, independent of grain structure.

29

4. SOLID-PHASE EPITAXIAL GROWTH OF Si FROM METAL/(POLY) Si SYSTEMS

Precipitation and epitaxial regrowth have been investigated in a number of systems, including Al/Ge(poly)/Ge, Si(amorphous)/Ag,[21,22] Al/Si(poly)[17] and others. In general, it has been proposed[23] that the formation of crystalline precipitates or regrowth structures proceeds through the following steps: 1) dissolution of the semiconductor by the metal film, 2) transport to a nucleation site, and 3) subsequent growth of crystallites. In all cases, detailed descriptions of mechanisms or controlling parameters were left underfined.

In the case of Al films in contact with polycrystalline Si films, the morphology of the final structure has been shown to depend upon the relative thicknesses, t, of the as-deposited Al and Si layers. For Al/Si(poly) systems heated below the eutectic temperature, the development of regrowth structures is shown schematically in Figure 14. When $t_{Al} < t_{Si}$, the Si precipitates in the Al film are constrained to grow in a lateral direction until an almost continuous film of Si crystallites are formed at the surface. For $t_{Al} < t_{Si}$, direction until an almost continuous film of Si crystallites are formed at the surface. For $t_{Al} > t_{Si}$, distinct crystallites are formed within the Al matrix until the Si has been consumed. The Al then occupies the area of the displaced Si and small pillarlike bridges connect the crystallites and substrate.

To extend these results and to examine further the correlation with film structure, we conducted a series of experiments on Al layers on poly-Si. From these experiments, we can propose a tentative model, shown schematically in Figure 15.

For the structure shown, the grain size of the evaporated Al film exceeds the average grain size of the chemical vapor deposited (CVD) poly-Si (Figures 16 and 17). Upon heating, interdiffusion is initiated rapidly at the smaller poly-Si grain boundaries and within the interior of the larger Al grains and poly-Si grains. Dislocation lines and other defects generated during (or subsequent to) growth of the films contribute to the enhanced interdiffusion of Si and Al. Simultaneously, Si is transported along the grain boundaries of the Al film. The Si transported and deposited along the Al grain boundaries will form the nucleation and growth sites for the Si crystallites. The Al forms
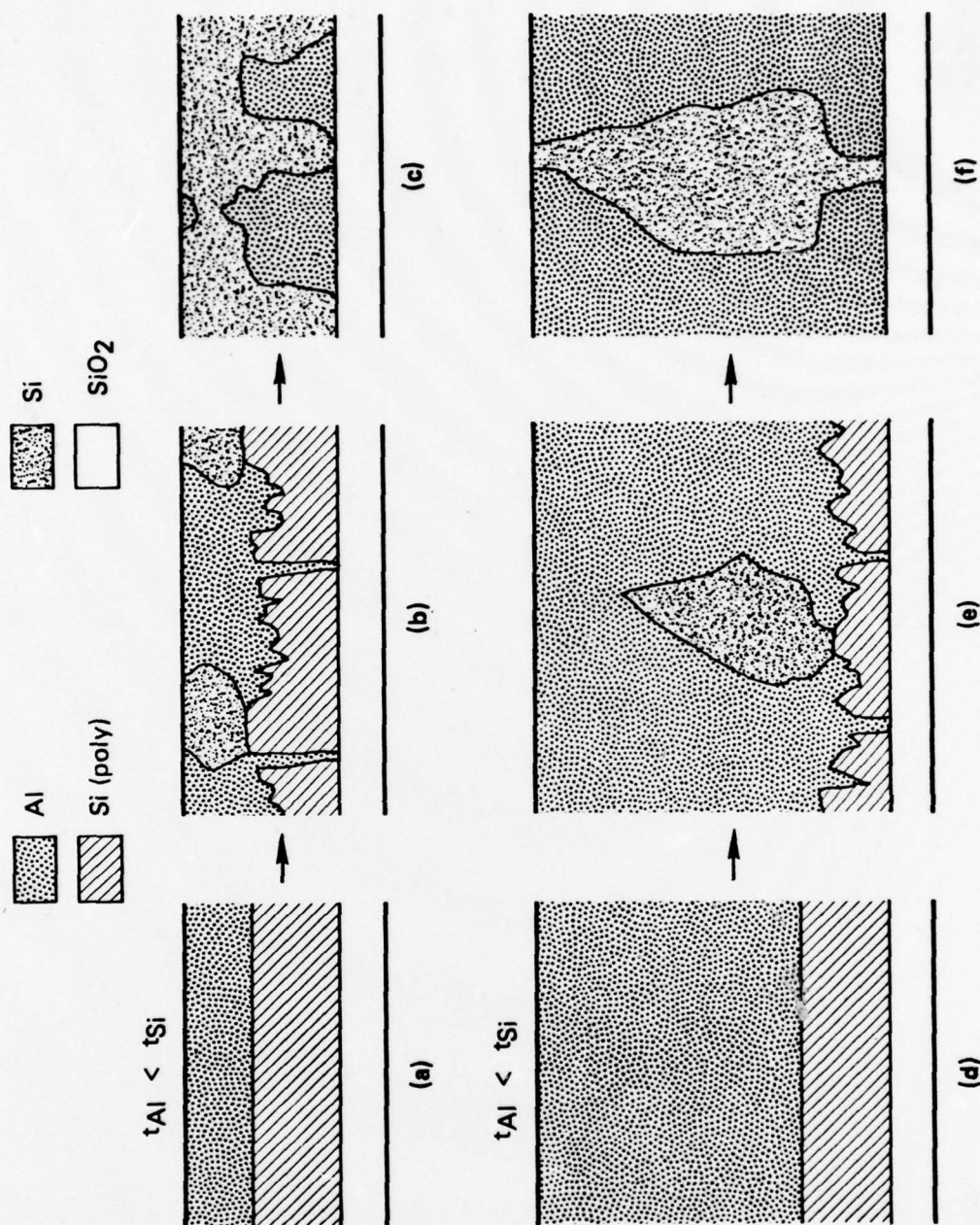
FIGURE 14. SCHEMATIC DIAGRAMS SHOWING THE CHANGES WHICH OCCUR DURING ANNEALING FOR SAMPLES WITH ORIGINAL Al LAYER THINNER THAN THE POLY Si LAYER [(a), (b), and (c)] AND FOR SAMPLES WITH ORIGINAL Al LAYER THICKER THAN THE POLY Si LAYER [(d), (e), and (f)] [AFTER NAKAMURA ET AL, REF. 17]
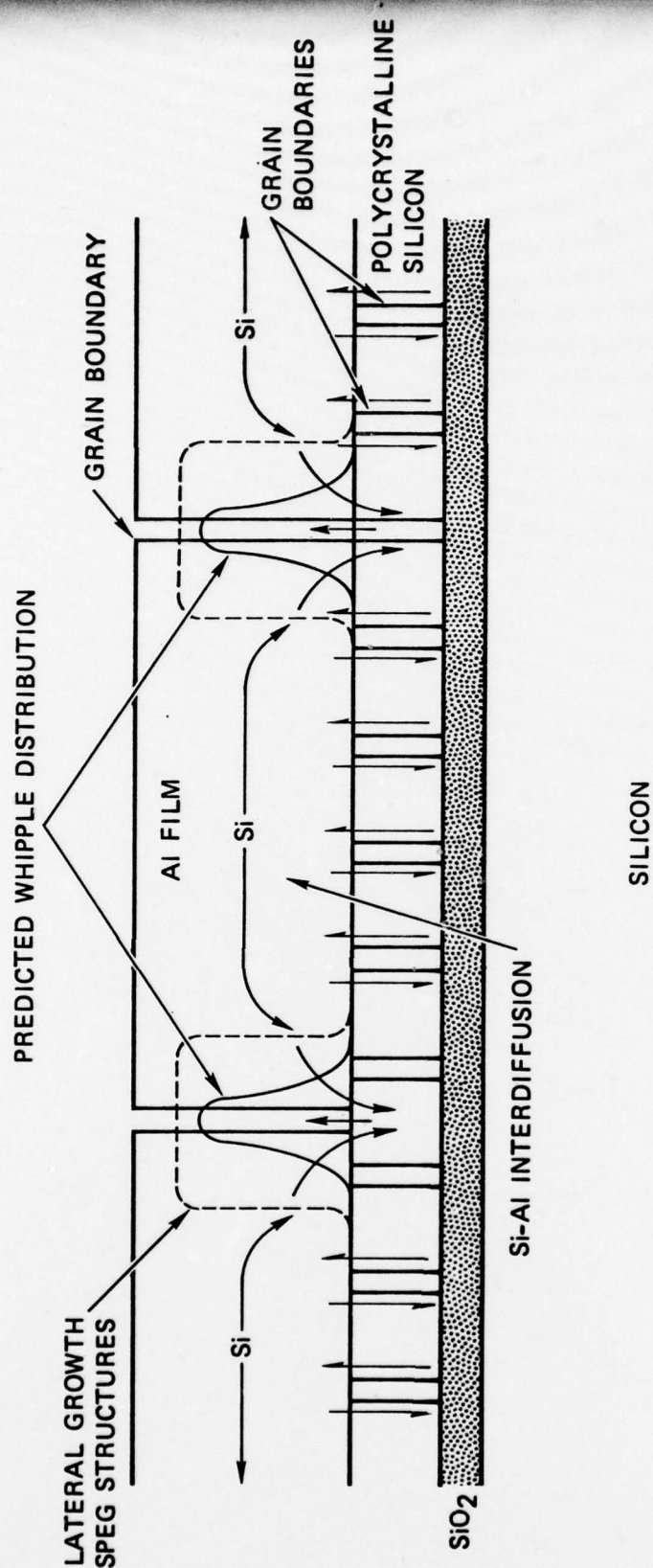
31

Figure 15. SCHEMATIC OF GRAIN BOUNDARY NUCLEATION AND GROWTH MODEL FOR
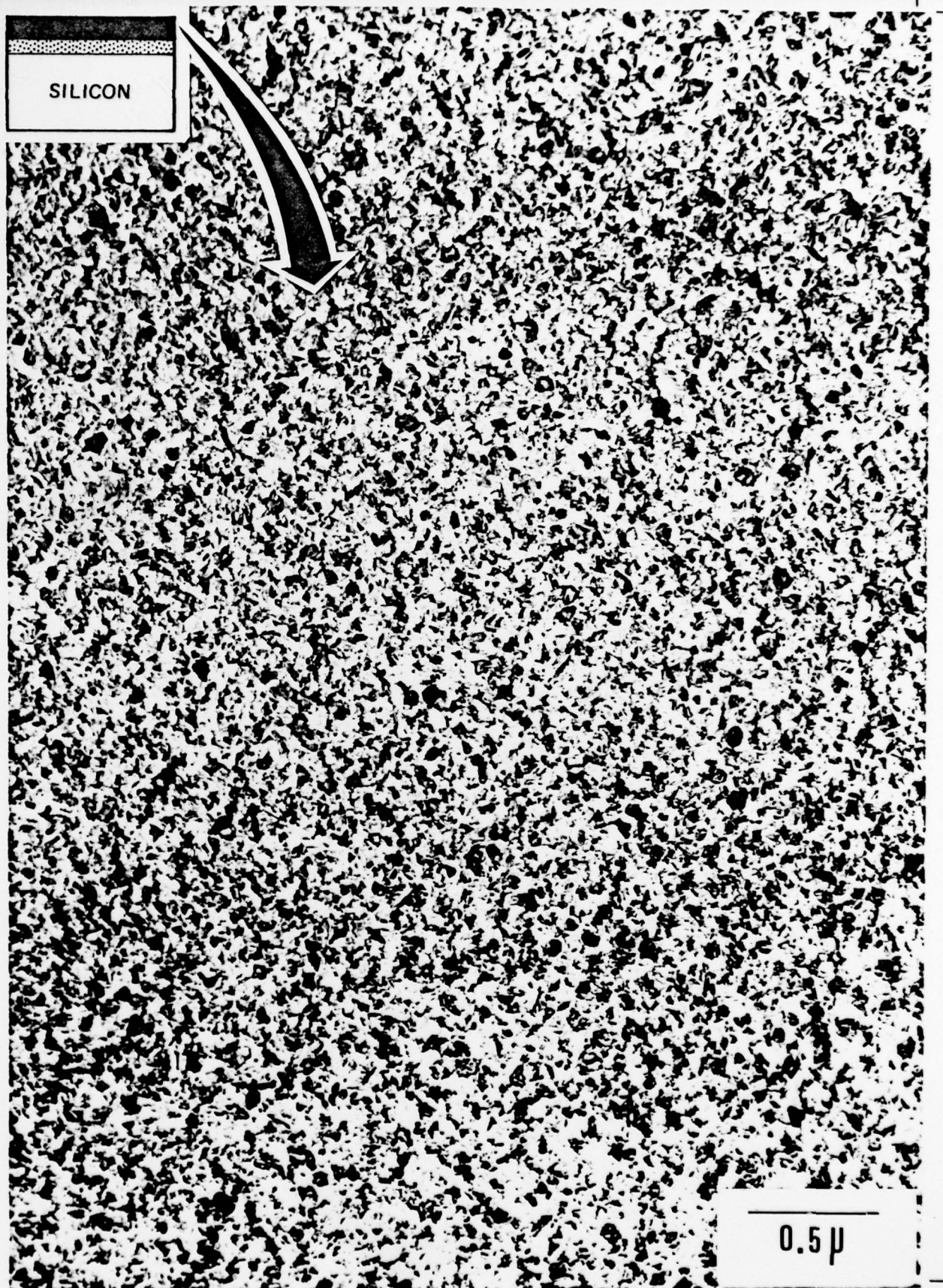SOLID-PHASE EPITAXIAL GROWTH IN THE Al/Si SYSTEM.

SILICON

0.5 μ

FIGURE 16. TRANSMISSION ELECTRON MICROGRAPH OF POLY-Si FILM DEPOSITED (CBD)
AT ≃ 620°C UPON THERMALLY-OXIDIZED (1000 Å) LAYER OF ⟨100⟩
SILICON WAFER.

33
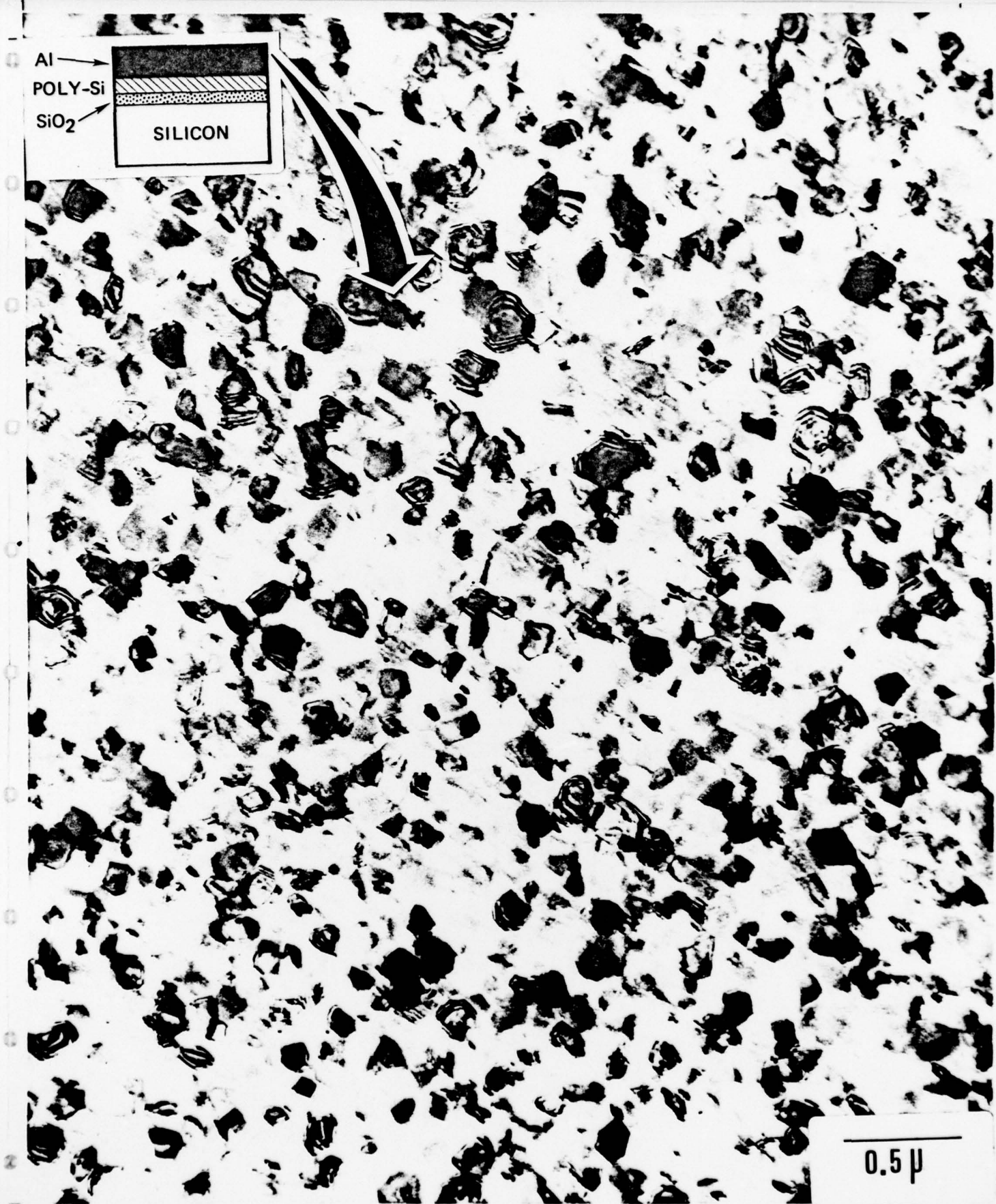
FIGURE 17. TRANSMISSION ELECTRON MICROGRAPH OF Al FILM IN Al/(poly)Si/
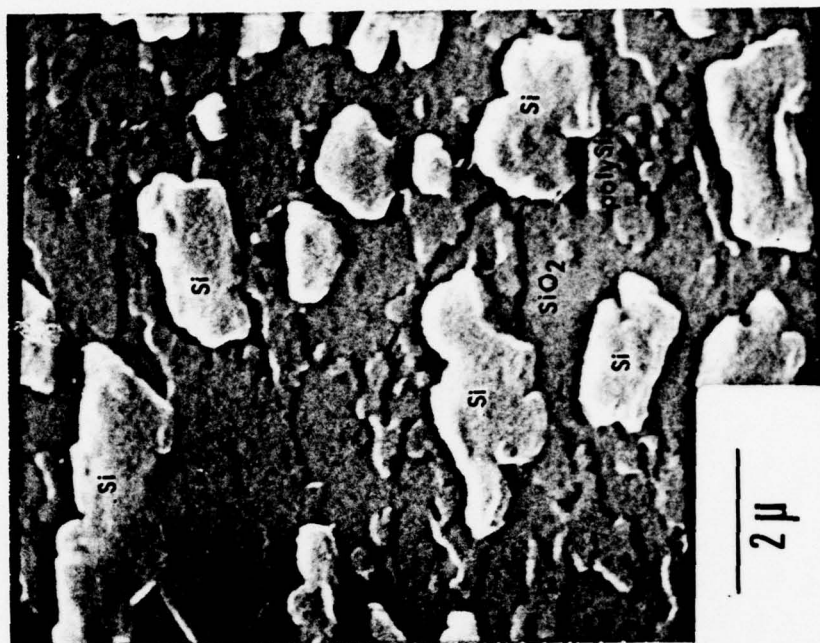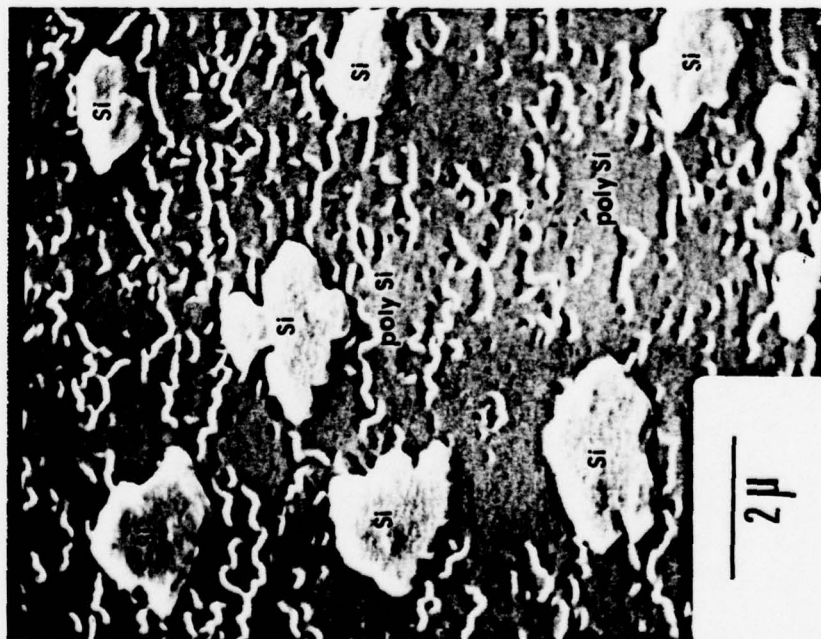SiO$_2$/Si STRUCTURE.

34

FIGURE 18. SCANNING ELECTRON MICROGRAPHS OF Al/Si/SiO₂ STRUCTURE AFTER ANNEALING AND ETCHING IN DILUTE HCl SOLUTION. a) 10 MIN. ANNEAL AT 450°C, b) 30 MIN. ANNEAL AT 450°C.

prominent Al/Si mixing zones or will move to the SiO_2 interface to occupy the position of the displaced Si. As the Al grains become saturated with Si upon further heating/cooling, Si atoms will move by defect-assisted diffusion or will be transported laterally along dislocation line cores (as shown in the previous section) to the grain boundary sites, where further growth and accretion occurs. The Si crystallites expand in a direction parallel to the film plane until the source of Si is depleted within the immediate region. Excess vacancies released at the grain boundary will also contribute to the enhanced lateral diffusion of Si and aid in the growth of Si crystallites at the grain boundary.

If $t_{Al} > t_{Si}$, the amount of available Si will be quickly depleted and further lateral gorwth of the Si crystallites terminated. The resulting structure will then consist of isolated Si crystallites in an Al matrix. If $t_{Al} < t_{Si}$, the available Si supplied by interdiffusion is not readily exhausted and lateral growth will continue until a coalesced, nearly continuous Si film is formed at the surface. Al will occupy the sites of displaced Si.

To further support this model, we show representative SEM data (Figure 18) obtained on Al/Si(poly) structures after heat-treatment at $450^{o}C$ for 10 minutes and 30 minutes and subsequently being etched in a dilute HCl solution. The poly-Si layers were formed by CBD at $620^{o}C$ on 1000 Å of SiO_2. The Al films were vacuum deposited onto the poly-Si by e-beam evaporation. Upon exposing the heated Al/Si structures to the HCl solution, Al and mixed Al-Si zones were etched and the Si remained intact.

In Figure 18a, we observe that after heating for 10 minutes, a large number of initial dissolution sites within the underlying poly-Si layer are developed. The average size of these zones approaches the average dimensions of grains within the Si film. Lateral undercutting into the Si(poly) beneath the Si crystallites shows that the Si crystallite is a distinct growth structure and not connected to the SiO_2 substrate. The support structure is instead composed of remnants of the poly-Si film, as shown diagrammatically in Figure 19.

After heating for 30 minutes (Figure 18b), the number of Si crystallites increases and the average size of etch structures in the poly-Si layer is also larger. Due to the fact that an HCl etch will remove both Al and Al-Si mixing regions, it is apparent that prominent interdiffusion has occurred between the

36

initial Al grains and portions of the Si layer. Since dissolution is initiated at the surface of the Al film, the structure of the overlying grains of Al layer will be formed in interdiffusion zones of the poly-Si layer, thereby providing an etched outline of larger Al grains at the surface. The distribution of grain sizes determined from the etch structures is in exact agreement with average saturation grain growth size determinations from correlated TEM examinations of the Al surface layer. This novel etching feature can then be used advantageously to determine the relationship between Al grains, interdiffusion zones, and Si regrowth structures. An examination of Figure 18b shows that the regrowth structures are formed at the intersection of two or more Al grain boundaries (Figure 20) in zones where prominent intermixing has occurred between the Si and Al layers, thereby providing additional support for the grain boundary nucleation and growth model.

To further investigate the mechanism of Si regrowth, we prepared a series of annealed Al/Si structures for TEM/TED examination. Using a three stage (back surface) jet thinning technique, we were able to successfully isolate the Al film from the remaining substrate structure. Careful TEM/TED analysis showed that Si regrowth structures were formed at grain boundary intersection points, in agreement with SEM data. Adjacent grains were highly defective, containing both dislocation lines and Si precipitates.

The data obtained from correlated experiments tend to support the tentative model proposed and further emphasize the significance of grain structure and grain boundaries in relation to solid phase regrowth. However, a number of important questions remain unanswered. If grain boundaries within both the semiconductor layer and metal transport layer serve as initiation sites for mass transport, as suggested by the experimental data, then the grain size ratio, g(metal)/g(semiconductor), should influence the kinetics of regrowth. For $g_m/g_s < 1$, transport and interdiffusion of mass across the metal/semiconductor interface should possibly be dominated by bulk grain diffusion. If $g_m/g_s \rightarrow 1$, it is not known whether separate large discrete crystallites of the metal will be formed on the SiO_2 substrate, in addition to the expected formation of crystallites of the semiconductor at the surface.

In earlier investigations, it was speculated that the ratio of the metal layer thickness to semiconductor grain size would be a critical parameter in
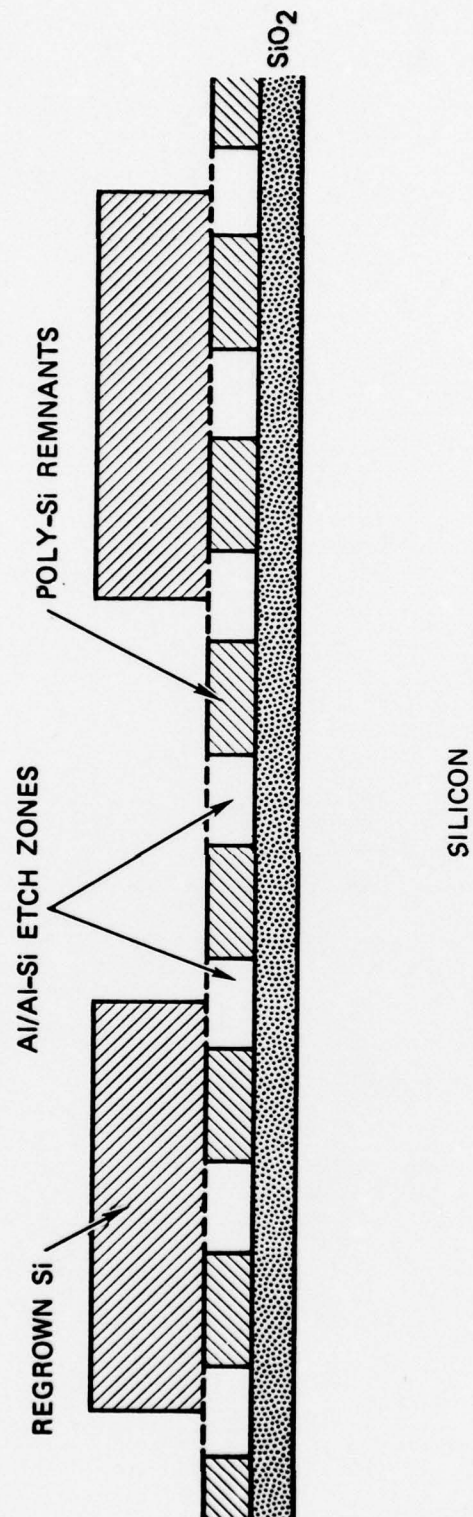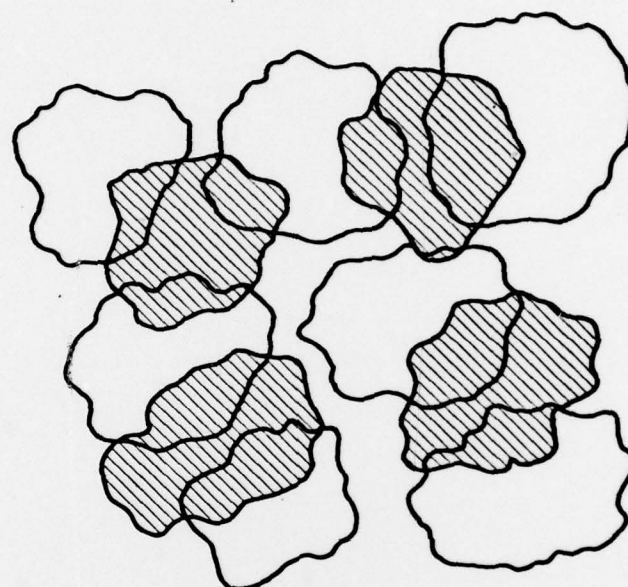
Figure 19. CROSS SECTION OF ETCHED ZONES AND Si REGROWTH
STRUCTURES SHOWN IN FIGURE 8a.

38

Si REGROWTH STRUCTURES

ETCH STRUCTURES IN
POLYCRYSTALLINE Si FILM

FIGURE 20. SCHEMATIC OF ETCHED ZONES AND Si REGROWTH STRUCTURES
SHOWN IN FIGURE 8b.

39

determining regrowth. Hence, if $t_m/g_s < 1$, recrystallization was said to be improbable. However, our experiments have shown that for $t_m/g_s = 1$ recrystallization occurs readily essentially independent of the thickness-to-grain-size ratio. For the case of metal layers on single crystal Si ($t_m/g_s \rightarrow 0$), regrowth of structures at grain boundaries is also consistent with recrystallization (as discussed in the previous section) and the grain boundary nucleation and growth model. In this case, the bounding layer is a single crystal and regrowth is in the form of expected tetrahedral or lineated features. For $t_m/g_s \gg 1$, as is typically encountered in semiconductor device applications, the system is somewhat more complicated, since the thick metal layer is usually not composed of a single layer of metal grains but a multiple stacking of layers.

From the data obtained thus far, it is apparent that it is not only the relative film thicknesses of the metal transport layer and polycrystalline semiconductor that determine the final morphology and development of epitaxial regrowth structures, but also the relative size of grain boundaries and defect concentrations within the two films.

If the kinetics of mass transport across the Al/Si interface is, indeed, partially dependent upon the concentration of microstructural defects within the films, it is conceivable that ion implantations could be used constructively in creating controlled defect populations within an annealed poly-Si layer prior to deposition of the Al film.

If defects aid in the lateral transport of Si within the Al film, implantation of protons during annealing should also aid in the regrowth of Si crystallites by providing vacancy-enhanced diffusion across the Al grains. Additionally, transport across the Al/Si interface can be accelerated by implanting Si or protons into the Si film prior to annealing.

REFERENCES

1. A. Hiraki, M. A. Nicolet, and J. W. Mayer, Appl. Phys. Lett. 18, 178 (1971).

2. A. Hiraki and E. Lugujjo, J. Vac. Sci. Techol. 9, 155 (1972).

3. A. Hiraki, E. Lugujjo, M. A. Nicolet, and J. W. Mayer, Phys. Status Solidi (A) 7, 401 (1971).

4. A. Hiraki, E. Lugujjo, and J. W. Mayer, J. Appl. Phys. 43, 3643 (1972).

5. A. K. Green and E. Bauer, J. Appl. Phys. 47, 1284 (1976).

6. M. Thackray, "Autoradiography of Photographic Images," Australian Atomic Energy Commission Tech. Rpt. No. AAEC/E317 (September 1974).

7. M. Thackray, D. Roman, E. L. R. Hetherington, and H. R. Brian, "Intensification of Photographs by Means of Autoradiography," Intl. J. Appl. Radiation and Isotopes 23, 79 (1972).

8. T. J. Magee, J. Peng, M. Thackray and R. Pettijohn, "Radioisotopic Image Enhancement Techniques for Electron Diffraction Data Analysis," (to be published, 1978).

9. G. A. Anderson, J. L. Bestel, A. A. Johnson, and B. Post, Mater. Sci. Engr. 7, 83 (1971).

10. T. R. Anatharaman, H. L. Luo, and W. Klement, Jr., Nature 210, 1040 (1966).

11. S. M. Sze, Physics of Semiconductor Devices, (John Wiley, New York, 1969), pp. 393-399.

12. J. D. Van Otterloo and L. J. Gerritsen, J. Appl. Phys. 49, 723 (1978).

13. J. O. McCaldin and H. Sankur, Appl. Phys. Lett. 20, 171 (1972).

14. H. Sankur, J. O. McCaldin and J. Devaney, Appl. Phys. Lett. 22, 64 (1973).

15. J. S. Best and J. O. McCaldin, J. Appl. Phys. 46, 4071 (1975).

16. C. J. Kircher, J. Appl. Phys. 47, 5394 (1976).

17. K. Nakamura, M. A. Nicolet, J. W. Mayer, R. J. Blattner and C. A. Evans, Jr., J. Appl. Phys. 46, 4678 (1975).

18. P. A. Totta and R. P. Sopher. IBM J. Res. Dev. 13, 226 (1969).

19. G. J. van Gurp. J. Appl. Phys. 44, 2040 (1973).

20. T. M. Reith and M. J. Sullivan, Appl. Phys. Lett. 32, 177 (1978).

21. G. Ottaviani, D. Sigurd, V. Marello, J. W. Mayer, and J. O. McCaldin, J. Appl. Phys. 45, 1730 (1974).

22. D. Sigurd, G. Ottaviani, H. J. Arnal, and J. W. Mayer, J. Appl. Phys. 45, 1740 (1974).

23. D. Sigurd, G. Ottaviani, V. Marrello, J. W. Mayer, and J. O. McCaldin, J. Non-Crystal. Solids 12, 135 (1973).

APPENDIX A – PUBLICATIONS AND TECHNICAL REPORTS

Publications

A-1. T. J. Magee and J. Peng, "Si Epitaxial Regrowth and Grain Structure of Al Metallization on (100) Si," J. Appl. Phys. <u>49</u>, 4284 (1978).

A-2. T. J. Magee and J. Peng, "Investigation of Solid-Solid Reactions of Au Films on Silicon," Phys. Stat. Sol. (A), Oct., 1978.

A-3. T. J. Magee and J. Peng, "Grain Boundary Nucleation and Solid Phase Regrowth in the Al/Polycrystalline Si System," (to be published in J. Appl. Phys. (1978).

A-4. T. J. Magee, J. Peng, M. Thackray and R. Pettijohn, "Radioisotopic Image Enhancement Techniques for Electron Diffraction Data Analysis," (to be published, 1978).

Technical Reports

A-5. T. J. Magee and J. Peng, "Application of Radioisotopic Image Enhancement Techniques to Metal/GaAs Reactions." ARACOR TNG-1, 1978.

A-6. T. J. Magee and J. Peng, "Investigation of Si/SiO_2 Interfaces Using RIE Techniques," ARACOR TN6-2, 1978.